Depth-selective 2D-ACAR studies on low-k dielectric thin films

S.W.H. Eijt[a],*, A. van Veen[a], C.V. Falub[a], R. Escobar Galindo[a], H. Schut[a], P.E. Mijnarends[a], F.K. de Theije[b], A.R. Balkenende[b]

[a] *Interfaculty Reactor Institute, Delft University of Technology, Mekelweg 15, NL-2629 JB, Delft, Netherlands*
[b] *Philips Research Laboratory, Inorganic Materials and Processing, Prof. Holstlaan 4, NL-5656 AA, Eindhoven, Netherlands*

Abstract

Depth-selective 2D-ACAR investigations on ordered mesoporous silica thin films provide direct evidence that *para*-positronium (*p*-Ps) created deep in the films can escape through a network of interconnected pores. The depth dependence of the escape fraction and of the average kinetic energy of non-thermally excited *p*-Ps is in quantitative agreement with Monte Carlo modeling, assuming classical collisions of *p*-Ps with the pore walls. The model provides insight in the shape of the angular correlation distributions and their sensitivity to, e.g., the effective wall mass M_s and pore dimensions.

© 2003 Elsevier Ltd. All rights reserved.

Keywords: Non-thermal positronium; 2D-ACAR; Mesoporous film; Effusion; Percolation; Depth profiling

1. Introduction

Thin films with a low dielectric constant ($k < 2.2$) are required for future generations ICs in order to substitute the present dielectric materials in ULSI devices. In order to lower the dielectric constant sufficiently, a high porosity of the material is needed. To facilitate integration issues, the pores should be smaller than about 5–10 nm.

One of the most suitable techniques for investigating the porosity of these thin films is positron depth profiling (Coleman, 2000; Petkov et al., 2001; Gidley et al., 1999; Rodbell et al., 2001; Sun et al., 2001). In this technique monochromatic positrons with energies between 100 eV and 30 keV are implanted in a thin layer and, after slowing down, annihilate with electrons in that layer. Previous positron studies with Doppler broadening, *ortho*-Ps (*o*-Ps) 3γ decay, and lifetime

measurements showed the excellent capability of this technique to investigate the cavity sizes and percolation thresholds. Complementary two-dimensional angular correlation of annihilation radiation (2D-ACAR) studies may provide further insight through *para*-positronium (*p*-Ps) investigations of such films. However, the lack of an intense variable energy positron beam for depth selectivity in the (sub-)μm range have limited such studies until now (Gessmann et al., 2001). Such a beam is now available in our institute (van Veen et al., 2001; Falub et al., 2001, 2002; Eijt et al., 2001).

In Doppler studies (Escobar Galindo et al., 2003; van Veen et al., 2003) connected with the work presented below, low-k silica films with ordered pore structures were studied systematically as a function of pore size, porosity, and hydrophilicity of the internal pore walls. The combination of Doppler and 3γ *o*-Ps decay depth-profiles and 2D-ACAR results (see also Escobar Galindo et al., 2001, 2003; van Veen et al., 2003) reveals that in a number of these samples, depending on the values of these parameters, Ps may escape from the layer through a network of interconnected pores. Preliminary results of *p*-Ps effusion for one of the samples were

---

*Corresponding author. Tel.: +31-15-2789053; fax: +31-15-2786422.

E-mail address: eijt@iri.tudelft.nl (S.W.H. Eijt).

shown by van Veen et al. (2003). Selected samples from these series were studied by 2D-ACAR in order to investigate the positronium effusion, which will be discussed here in more detail.

2. Experimental

The thin film mesoporous silica sample discussed here was produced from a solution containing silicon alkoxides (TEOS and MTMS) and a surfactant (Pluronic F127) (Escobar Galindo et al., 2003). The molar ratio TEOS/MTMS = 1 used results in a hydrophobic pore wall surface because methyl end groups are incorporated in the walls (Escobar Galindo et al., 2003). A layer thickness of 1327 nm and a porosity of 57% have been obtained from ellipsometry. The pores are highly uniform and form an ordered mesophase with 2D hexagonal packing of cylinders with a diameter of about 5 nm lying flat in the plane of the surface. The porous SiO_2 layer has a density $\rho = 1.0\,g/cm^3$ and is situated on top of a Si(1 0 0) substrate.

A depth-selective 2D-ACAR study was performed with the intense variable energy positron beam POSH (van Veen et al., 2001). Six 2D-ACAR distributions were obtained for positron implantation energies between 0.5 and 11 keV, i.e., between average implantation depths of $\sim 15\,nm$ and $\sim 2\,\mu m$. The momentum resolution was $1.4 \times 1.4 (10^{-3} m_0 c)^2$, where m_0 is the electron rest mass and c the velocity of light.

3. 2D-ACAR study

Fig. 1 shows representative 2D-ACAR cross-sections at positron energies of 1.5 and 5.0 keV (i.e., at average implantation depths of ~ 75 and $\sim 520\,nm$, respectively) for momenta perpendicular (p_y) and parallel (p_x) to the sample surface. A pronounced off-center profile is obtained in the p_y direction, as a result of p-Ps particles which escape from the low-k thin film with a non-zero average velocity along p_y. The shift in the maximum of the distribution along p_y shows a gradual decrease with depth, resulting both from a reduction of the average momentum of the p-Ps particles flying off and from a decrease in their fraction.

3.1. Gas effusion model analysis

The data were analyzed using a simple gas effusion model, which describes the escape of gas atoms from a closed box through a small hole (Escobar Galindo et al., 2001; Reif, 1987). This model correctly describes the distributions for some of the samples (van Veen et al., 2003; Escobar Galindo et al., 2001), although it should be noted that the condition of a collection of gas (Ps) atoms at thermal equilibrium is clearly not met in the experiment. We assume an isotropic Maxwellian momentum distribution in the final pore before escape from the layer, and a $\cos\theta_0$ emission profile, in which θ_0 is the emission angle relative to the surface normal. This gives the following projected momentum density $dN(p_x, p_y)$
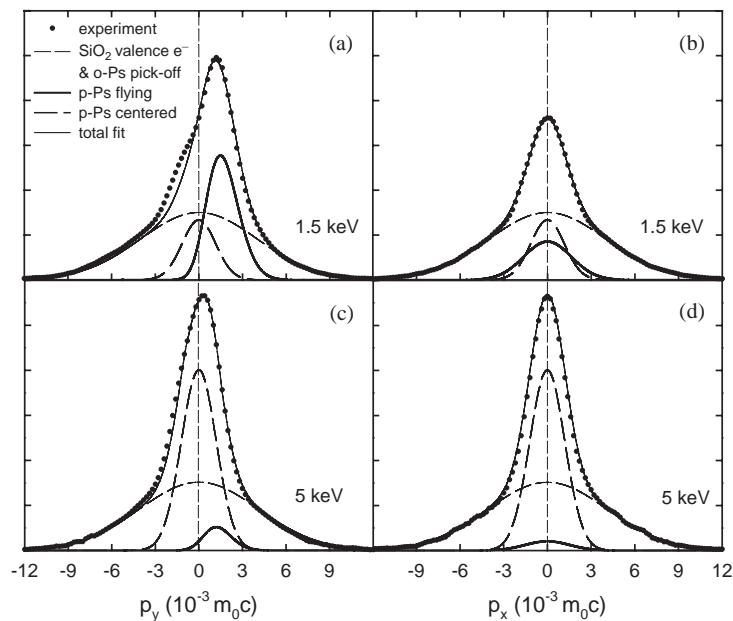

Fig. 1. 2D-ACAR cross-sections at 1.5 keV along (a) the p_y (p-Ps effusion) direction and (b) p_x direction. (c) and (d): same as (a) and (b), but for 5.0 keV. The full curves are fits using a gas effusion model (see text).

for the escaping p-Ps:

$$dN(p_x, p_y) = N_0[p_y \exp(-p_y^2/p_0^2)] dp_y$$
$$\times [\exp(-p_x^2/p_0^2)] dp_x, \quad (1)$$

in which N_0 is the number of p-Ps escaping from the sample, and $\sqrt{(3/2)}p_0$ is the root-mean-square average momentum of the p-Ps particles in the final pore before escape. The average kinetic energy in the final pore is obtained from $\langle E \rangle_{fly} = (3/2)p_0^2/2m_{Ps}$, where m_{Ps} is the p-Ps mass. The centro-symmetric contributions from p-Ps and from amorphous SiO_2 and o-Ps pick-off (FWHM of $\sim 9.5 \times 10^{-3} m_0 c$) were modeled by two Gaussians. Although the main features can be described by the model, a clear discrepancy with the data is apparent at low positron implantation energies (Fig. 1), in the range around $-1.5 \times 10^{-3} m_0 c$ along the p_y direction. The deviation gradually disappears for larger positron implantation energies (average depth), and will be discussed below.

3.2. Observed p-Ps average energy and fractions

The average energy $\langle E \rangle_{fly}$ and fractions of the two p-Ps components obtained are given in Figs. 2 and 3(a), respectively. The average energy ranges between $\langle E \rangle_{fly} \sim 0.4$ eV for p-Ps created deep in the layer and $\langle E \rangle_{fly} \sim 0.85$ eV close to the surface, i.e. both substantially larger than the expected thermal kinetic energy of $3/2k_B T = 38$ meV at room temperature. Therefore, the p-Ps particles, after being emitted from the pore walls at

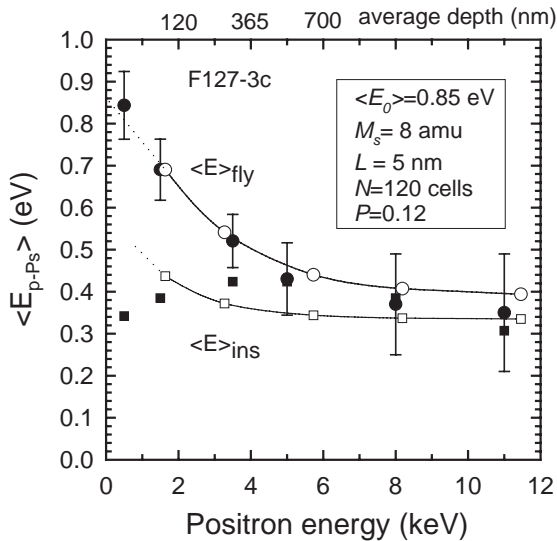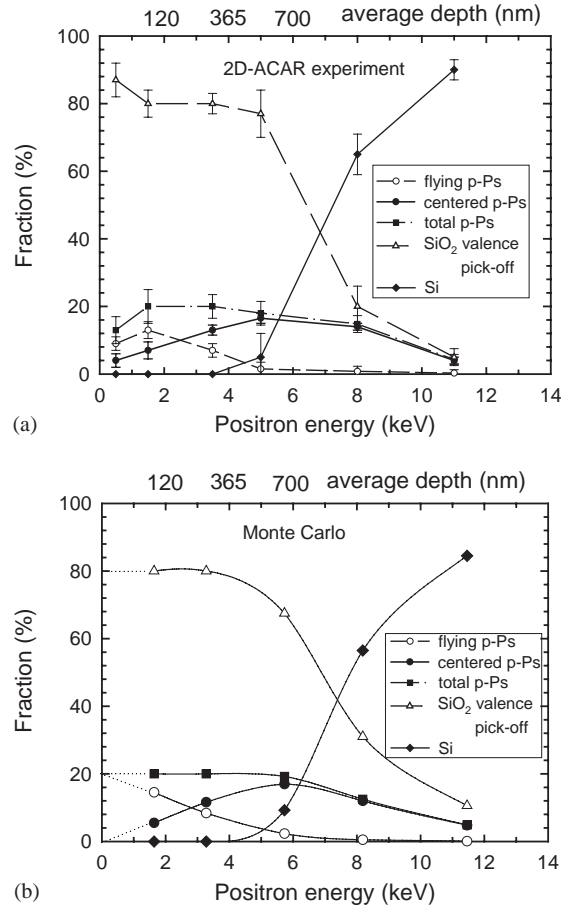Fig. 3. Para-positronium fractions from 2D-ACAR experiments on the low-k sample studied. (a) Experimental total p-Ps fraction (filled squares) as a function of positron implantation energy (i.e., average depth); fraction of annihilations stemming from p-Ps escaping from the thin low-k layer into the vacuum (open circles); fraction of p-Ps annihilations inside the low-k layer (filled circles). The open triangles denote annihilations with valence electrons of the SiO_2 wall material (including o-Ps pick-off); filled diamonds represent annihilations with a Si(1 0 0) signature from the substrate and the interface. The average implantation depth in the low-k layer is shown. (b) Results from the Monte Carlo model with parameters $\langle E_0 \rangle = 0.85$ eV, $M_s = 8$ amu, $L = 5$ nm, $P = 0.12$, $N = 120$ cells in the low-k layer (see text).

Fig. 2. Average energy vs. positron implantation energy for p-Ps flying off the low-k layer $\langle E \rangle_{fly}$ (experiment—filled dots, Monte Carlo model—open dots) and for p-Ps annihilating inside the layer $\langle E \rangle_{ins}$ (experiment—filled squares, Monte Carlo model—open squares). The average implantation depth in the low-k layer is shown.

~ 0.85 eV, do not interact sufficiently with the porous SiO_2 before their escape to reach thermal equilibrium. A strong reduction in $\langle E \rangle_{fly}$ as a function of the average implantation depth is observed, which saturates beyond a positron energy of ~ 6 keV. This is accompanied by a clear decrease in the fraction of escaping p-Ps. Simultaneously, the fraction of p-Ps annihilating inside the low-k layer shows a corresponding increase of about the same size. This component is most likely to come from
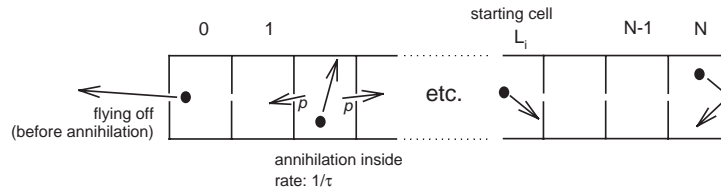
Fig. 4. Schematic Monte Carlo model geometry for studying p-Ps out-diffusion through an ordered network of connected pores, including annihilation before escape.

annihilations in the large cylindrical pores of the layer. Namely, both the total p-Ps fraction and the observed o-Ps 3γ annihilation fraction (van Veen et al., 2003; Escobar Galindo et al., 2003) remain approximately constant in the range between 1 and 5 keV, indicating a constant porosity of the layer. Moreover, the FWHM of the centered p-Ps contribution of $\sim 2.6\,10^{-3}m_0c$ is significantly smaller than typical values for p-Ps in the micropores of amorphous SiO_2 (e.g. Peng et al., 1996). Using the conversion method of Nakanishi and Jean (1988), i.e., assuming thermal p-Ps, the FWHM indicates pore sizes of ~ 1.5 nm, instead of the commonly observed size of ~ 0.9–1.1 nm. Moreover, wall thicknesses are about 1.5 nm only, limiting the probability of finding large closed pores in the walls. On the other hand, the thin walls are expected to be permeable to Ps. Therefore, we attribute the centered component to non-thermal p-Ps as well, namely those p-Ps atoms annihilating inside the large pores prior to escape.

4. Monte Carlo model

In order to gain some insight in the interaction of p-Ps with the pores, a Monte Carlo approach was followed to model p-Ps motion through an effectively one-dimensional pore chain (see Fig. 4). In the Monte Carlo procedure, typically 20,000 p-Ps particles are used, each of which are subsequently positioned in one of the N cells according to a Makhovian implantation profile given by the positron implantation energy. A layer thickness of ~ 1.1 μm was used, as obtained from VEPFIT analysis (van Veen et al., 1990). After creation at an initial energy E_0, the p-Ps particle subsequently experiences energy losses through collisions with the walls according to $\Delta E = 4m_{Ps}/M_s \cos^2\theta E(t)$, in which M_s is the effective wall mass, θ the angle of incidence of the p-Ps particle relative to the wall normal, and $E(t)$ the kinetic energy at time t. For closed pores, Nagashima et al. (1995) describes the time evolution of the kinetic energy in more detail. An effective scattering length L is used.[1] The number of cells N is $N = 120$ for $L = 5$ nm,

obtained from $N((3/2)L + d_{wall}) = 1.1$ μm, with a wall thickness $d_{wall} \sim 1.5$ nm. During each time step $\Delta t = L/v(t)$, with $v(t)$ the Ps velocity, the p-Ps has a finite probability to annihilate at a rate $\lambda = \Delta t/\tau$, with $\tau = 125$ ps. To model the diffusion through the porous layer via permeable pore walls, at each collision the particle is given a probability P to move from the nth cell to either cell $n+1$ or to cell $n-1$, after which θ is changed randomly.

When entering cell $n = 0$, the p-Ps particle is assumed to escape from the porous layer with the kinetic energy it has at that moment. Energy distributions were sampled in intervals $\delta E = 0.04$ eV, using the calculated energies, E_{fly} or E_{ins}, of the p-Ps atoms either escaping or annihilating in the layer.

5. Comparison and discussion

5.1. p-Ps average energy and fractions

The depth-dependence of the energy distribution and the p-Ps fractions at annihilation has been calculated (Figs. 2 and 3b). An average initial energy $\langle E_0 \rangle = 0.85$ eV with a Gaussian spread of 0.35 eV FWHM, inferred from previous time-of-flight measurements on Ps emitted by quartz surfaces (Nagashima et al., 1998) and from 2D-ACAR studies of silica aerogel (Nagashima et al., 1995), has been assumed. It was found that a satisfactory agreement between the observed and modeled average energy $\langle E \rangle_{fly}$ vs. positron implantation energy is obtained (Fig. 2), by taking $M_s = 8$ amu, $L = 5$ nm and $P = 0.12$. The sharp initial decrease in $\langle E \rangle_{fly}$ is clearly a result of the increase in the average number of collisions before p-Ps can escape from the layer. The observed saturation at larger implantation energies is caused by (a) most p-Ps flying off originating in a limited subsurface depth range in the layer (see below), and (b) the shape of the implantation profile in the low-k layer changing only slowly with implantation energy. The model shows that the p-Ps annihilating inside the low-k layer has the expected lower average energy $\langle E \rangle_{ins}$ at annihilation, in reasonable agreement with the experimental data (Fig. 2).

---

[1] For simple pore geometries, such as spheres of diameter a, or cylinders of diameter and length a, the effective scattering length is $L = 2/3a$.

The Monte Carlo model has been used to obtain the fractions (Fig. 3b). It is assumed that (1) a constant 20:80 ratio for the total p-Ps vs. SiO_2 annihilations exists in the low-k layer, as indicated by the experiment, and (2) an interface layer is present at the boundary with the Si substrate (as clearly observed in Dopper experiments using S-W plots (van Veen et al., 2003), which contributes between ~ 5 and ~ 12 keV and at a fixed ratio to the observed p-Ps, SiO_2 and Si fractions. The fractions finally obtained (Fig. 3b) satisfactorily reproduce the experimental results. This demonstrates the validity of the applied Monte Carlo model. The fraction of p-Ps escaping is found to follow a near exponential decay with average implantation depth, with an effective escape depth in the sample of $L_{probe} = 300 \pm 20$ nm. We note from the model that o-Ps, assuming a lifetime τ in the material of $\sim 100 \tau_{p-Ps} = 12.5$ ns (vs. 142 ns in vacuum) by pick-off processes, is expected to have an approximately five (or ten) times larger escape depth, and can therefore be applied to probe thicker films. The model also allows an estimation of the Ps thermalisation time of 1.5 ns at $M_s = 8$ amu and $L = 5$ nm, defined here as the time at which the detected average energy $\langle E \rangle$ for closed pores would have decreased to 2×38 meV (see also Nagashima et al. (1995) for an analytical description of $\langle E \rangle(t)$).

5.2. 2D-ACAR shapes

The energy distributions obtained from the model can be converted into momentum distributions (Eijt et al., 2001; Nakanishi and Jean, 1988). A $\cos \theta_0$ emission profile is assumed for the p-Ps atoms escaping. It is then relatively straightforward to project the momentum distribution along an appropriate axis to obtain the 2D-ACAR cross-sections along the p_x and p_y directions. Typically, it was found that cross-sections along the direction of flying off are somewhat sharper than for a Maxwellian distribution (Eq. (1)). Further, the distributions of p-Ps annihilating inside the pores are broader and flatter than a Gaussian distribution. Clearly this will result in better fits in, e.g., Fig. 1. A more detailed comparison will be presented elsewhere.

5.3. Capping layer

We further studied the influence of depositing a 10 nm dense SiO_2 capping layer on top of the sample. The effusion component then disappears, whereas the centered p-Ps component increases correspondingly. In the range from 1.5 to 11 keV, the p-Ps component reveals an average kinetic energy of 0.34 eV, i.e., close to the value of 0.32 eV obtained with the Monte Carlo model using the same parameters as for the uncapped sample. This further confirms the validity of the Monte Carlo model used.
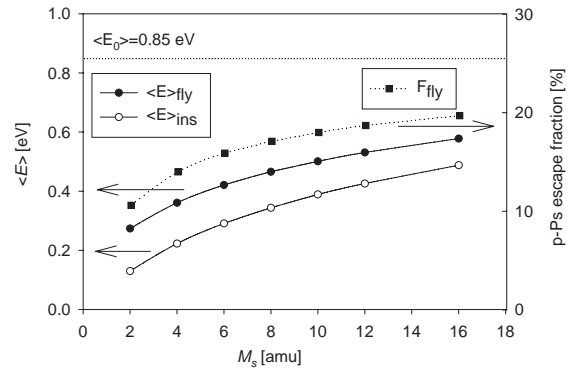

Fig. 5. Dependence of the average $\langle E \rangle_{fly}$, F_{fly} and $\langle E \rangle_{ins}$ at 3.5 keV on the effective wall mass M_s, using parameter values in the Monte Carlo calculations given before.

5.4. Effective mass and scattering length

Finally, the sensitivity of the p-Ps effusion on the various pore parameters can be predicted. For example, Fig. 5 shows the dependence of $\langle E \rangle_{fly}$ on the effective mass M_s at 3.5 keV. The effective mass can therefore be determined to within about 0.5 amu at $M_s = 8$ amu, whereas the escape fraction F_{fly} is somewhat less sensitive. Simulations show that the effective scattering length L yields a similar dependence (see also Nagashima et al., 1995).

In summary, the positron beam studies performed show that the investigation of variations in p-Ps 2D-ACAR distributions for samples with different types of molecular end groups at the pore walls (to vary their hydrophilic character) and with various pore dimensions are well accessible. Our studies have further shown that both a Monte Carlo approach as well as rate/diffusion theory for multiple energy groups (see van Veen et al., 2003) can be applied to the description of the positronium transport and cooling in the mesoporous layers.

6. Conclusions

We have used depth-selective positron 2D-ACAR to study p-Ps effusion in low-k dielectric SiO_2 thin films with ordered porosity, and show that p-Ps can escape from the nanoporous layer through a network of interconnected pores. A comparison is made with a Monte Carlo model assuming classical interactions between p-Ps, present at high kinetic energies, and the pore walls. The depth dependences of the observed average kinetic energy and the fraction of p-Ps are in quantitative agreement with the model. An effective p-Ps escape depth $L_{probe} = 300 \pm 20$ nm was deduced for the sample studied. The Monte Carlo model predicts

deviations in the 2D-ACAR shape from a simple gas effusion law, as has been experimentally observed in some of the mesoporous layers.

References

Coleman, P.G., (Ed.), 2000. Positron Beams and their Applications. World Scientific, Singapore.

Eijt, S.W.H., Falub, C.V., van Veen, A., Schut, H., Mijnarends, P.E., van Huis, M.A., Fedorov, A.V., 2001. Ion-implantation generated nanovoids in Si and MgO monitored by high-resolution positron beam analysis. Mater. Res. Soc. Symp. Proc. 647, O.14.11.1-6.

Escobar Galindo, R., Eijt, S.W.H., van Veen, A., Schut, H., Falub, C.V., 2001. Positron beam analysis of ordered mesoporous silica low-k dielectric thin films. IRI report IRI-DM-2001-005; and Eijt, S.W.H., Falub, C.V., van Veen, A., Escobar Galindo, R., Mijnarends, P.E., de Theije, F.K., and Balkenende, A.R., unpublished.

Escobar Galindo, R., van Veen, A., Schut, H., Eijt, S.W.H., Falub, C.V., Balkenende, A.R., de Theije, F.K., 2003. Systematic positron study of hydrophilicity of the internal pore surface in ordered low-k silica thin films. Mater. Sci. Eng. B, in press.

Falub, C.V., Eijt, S.W.H., van Veen, A., Mijnarends, P.E., Schut, H., 2001. Depth-selective 2D-ACAR with POSH: application to nanocavities generated by ion implantation. Mater. Sci. Forum 363–365, 561–563.

Falub, C.V., Eijt, S.W.H., Mijnarends, P.E., Schut, H., van Veen, A., 2002. Magnetic focusing of an intense slow positron beam for enhanced depth-resolved analysis of thin films and interfaces. Nucl. Instrum. Methods A 488, 478–492.

Gessmann, Th., Petkov, M.P., Weber, M.H., Lynn, K.G., Rodbell, K.P., Asoka-Kumar, P., Stoeffl, W., Howell, R.H., 2001. Study of positronium in low-k dielectric films by means of 2D-angular correlation experiments at a high-intensity slow-positron beam. Mater. Sci. Forum 363–365, 585–587.

Gidley, D.W., Frieze, W.E., Dull, T.L., Yee, A.F., Ryan, E.T., Ho, H.-M., 1999. Positronium annihilation in mesoporous thin films. Phys. Rev. B 60, 5157–5160.

Nagashima, Y., Kakimoto, M., Hyodo, T., Fujiwara, K., Ichimura, A., Chang, T., Deng, J., Akahane, T., Chiba, T., Suzuki, K., McKee, B.T.A., Stewart, A.T., 1995. Thermalization of free positronium atoms by collisions with silica-powder grains, aerogel grains, and gas molecules. Phys. Rev. A 52, 258–265.

Nagashima, Y., Morinaka, Y., Kurihara, T., Nagai, Y., Hyodo, T., Shidara, T., Nakahara, K., 1998. Origins of positronium emitted from SiO$_2$. Phys. Rev. B 58, 12676–12679.

Nakanishi, H., Jean, Y.C., 1988. In: Schrader, D.M., Jean, Y.C. (Eds.), Positron and Positronium Chemistry—Studies in Physical and Theoretical Chemistry, Vol. 57. Elsevier, Amsterdam, pp. 159–192.

Peng, J.P., Lynn, K.G., Asoka-Kumar, P., Becker, D.P., Harshman, D.R., 1996. Study of the SiO$_2$–Si interface using variable energy positron two-dimensional angular correlation of annihilation radiation. Phys. Rev. Lett. 76, 2157–2160.

Petkov, M.P., Weber, M.H., Lynn, K.G., Rodbell, K.P., Cohen, S.A., 2001. Open volume defects (measured by positron annihilation spectroscopy) in thin film hydrogen-silsesquioxane spin-on-glass; correlation with dielectric constant. J. Appl. Phys. 86, 3104–3109.

Reif, F., 1987. Fundamentals of Statistical and Thermal Physics. McGraw-Hill, Singapore, pp. 262–277.

Rodbell, K.P., Petkov, M.P., Weber, M.H., Lynn, K.G., Volksen, W., Miller, R.D., 2001. Current and potential uses of positron beams to study porosity in low-k dielectric thin films. Mater. Sci. Forum 363–365, 15–19.

Sun, J., Gidley, D.W., Dull, T.L., Frieze, W.E., Yee, A.F., Ryan, E.T., Lin, S., Wetzel, J., 2001. Probing diffusion barrier integrity on porous silica low-k thin films using positron annihilation lifetime spectroscopy. J. Appl. Phys. 89, 5138–5144.

van Veen, A., Schut, H., de Vries, J., Hakvoort, R.A., IJpma, M.R., 1990. In: Schultz, P.J., Massoumi, G.R., Simpson, P.J. (Eds.), Positron Beams for Solids and Surfaces. American Institute of Physics, New York, pp. 171.

van Veen, A., Schut, H., de Roode, J., Labohm, F., Falub, C.V., Eijt, S.W.H., Mijnarends, P.E., 2001. Intense positron sources and their applications. Mater. Sci. Forum 363–365, 415–419.

van Veen, A., Escobar Galindo, R., Schut, H., Eijt, S.W.H., Falub, C.V., Balkenende, A.R., de Theije, F.K., 2003. Positron beam analysis of structurally ordered porosity in mesoporous silica thin films. Mater. Sci. Eng. B, in press.